JSML
Journal of Science and Mathematics Letters
ISSN 2462-2052 • eISSN 2600-8718

Research Article

Coupled Effects of Viscoelasticity and Nanoparticle Dynamics on Mixed Convection of Brinkman Nanofluids

Farahanie Fauzi[1,2], Abdul Rahman Mohd Kasim[1]*, Siti Farah Haryatie Mohd Kanafiah[2], Nurizzatul Atikha Rahmat[3], Adeshina Taofeeq Adeosun[1,4], Nurul Amira Zainal[5], Livia Owen[6]

1 Centre for Mathematical Sciences, Universiti Malaysia Pahang Al-Sultan Abdullah, 26300 Gambang, Pahang, Malaysia
2 College of Computing, Informatics and Mathematics, Universiti Teknologi MARA Kelantan Branch, 18500 Machang, Kelantan, Malaysia
3 Faculty of Mechanical and Automotive Engineering Technology, Universiti Malaysia Pahang Al-Sultan Abdullah, 26300 Gambang, Pahang, Malaysia
4 Federal College of Education, 232102 Iwo, Nigeria
5 Faculty of Mechanical Technology and Engineering, Universiti Teknikal Malaysia Melaka, Hang Tuah Jaya, 76100 Durian Tunggal, Melaka, Malaysia
6 Center for Mathematics and Society, Faculty of Science, Parahyangan Catholic University, 40141 Bandung, Indonesia
* Corresponding author: rahmanmohd@umpsa.edu.my

ARTICLE HISTORY

Received
15 September 2025
Revised
25 January 2026
Accepted
17 February 2026
Published
1 April 2026

KEYWORDS

Convection
Brinkman
Nanofluid
Buongiorno
Viscoelasticity

ABSTRACT

Low thermal conductivity limits the effectiveness of conventional heat transfer fluids in industrial settings. Researchers have investigated modified fluid-based strategies to get around this. The mixed convection of a viscoelastic Brinkman nanofluid passing over a horizontal circular cylinder is examined in this work. The equations were simplified by using the Buongiorno nanofluid model and the necessary non-dimensional and similarity transformations. The Keller-Box Method (KBM), which is implemented in *Matlab* package, was then used to solve the equations numerically. In addition to the profiles of velocity, temperature, and nanoparticle volume fraction, numerical solutions are provided and analysed for the coefficient of skin friction, local Nusselt and Sherwood numbers, and the viscoelasticity, Lewis number, Brownian number, buoyancy ratio parameter, and thermophoresis parameter for each of the governing parameters. Numerical solutions are presented and analysed for the skin friction coefficient, local Nusselt number and Sherwood number alongside the profiles of velocity, temperature, and nanoparticle volume fraction for different governing parameters, specifically the viscoelasticity, Brownian number, buoyancy ratio parameter, and thermophoresis parameter. The numerical findings unequivocally indicate that an increase in the viscoelastic parameter results in a significant decrease in the skin friction coefficient, attributed to the inhibition of momentum diffusion near the cylinder surface caused by the elastic characteristic in the fluid.

https://doi.org/10.37134/jsml.vol14.2.1.2026

1. INTRODUCTION

Convection heat transfer is characterised as thermal transfer resulting from fluid motion. Fluids involved in convective heat transfer can be categorised into Newtonian and non-Newtonian types. Newtonian fluid adheres to Newton's law of viscosity, while a non-Newtonian fluid diverges from this principle. The most common Newtonian fluids include water, air, gasoline, and oils, whereas examples of non-Newtonian fluids include blood and liquid polymers (Çengel and Ghajar, 2020). The study of non-Newtonian fluids is more challenging than that of Newtonian fluids, as they deviate from Newton's law of viscosity. Nevertheless, such studies remain in demand due to their wide-ranging applications (Amera Aziz et al., 2019; Dey et al., 2020). One category of non-Newtonian fluid utilized in numerous essential applications is viscoelastic fluids, which demonstrate both viscosity and elasticity (Pérez-Reyes et al., 2018). Consequently, the mathematical model of viscoelastic fluid has been independently developed and resolved in numerous investigations over several decades since the 1960s.

Aside from using viscoelastic fluid, there are many other ways to improve heat transfer among many other things, it could mean diluting a substance in the fluid or changing the surfaces that the fluids interact with (Çengel and Ghajar, 2020). The employment of porous media is thought to improve heat transmission, as the porous surface expands the overall area in contact with the fluid, hence increasing the heat transfer rate (Ingham and Pop, 1998). Other than that, the utilisation of nanofluids and hybrid nanofluids is nowadays increasing, as these fluids are reported to enhance heat transfer by up to double compared to traditional fluids (Mahat et al., 2020). Nanofluid is formed when nanoparticles measuring between 1 to 100 nanometres are dispersed in a fluid (Li et al., 2021). These special benefits have led to the widespread usage of viscoelastic fluids and nanofluids in many different applications, including heat exchangers, solar thermal collectors, automobile heat management, cooling electronic equipment, and many more (Li et al., 2021). As industrial technology progresses, excessive heat in high-performance computers and engineering systems poses significant challenges. To improve cooling capacity and ensure stable operation, researchers have proposed nanofluids as advanced heat transfer media (Ahmed et al., 2018; Ali et al., 2014; Kumar et al., 2020). In solar energy systems, likewise, the efficiency of collectors and the thermal behaviour of the working fluid play a key role in maximizing energy output (Hussein, 2016). As a result, scientists started researching the working medium for heat transmission and discovered that nanofluids would be the best option (Elsheikh et al., 2018). Due to these huge applications, many studies on convective heat transfer related to nanofluid, viscoelastic fluid and porous medium have been performed, focusing on either free or mixed convection.

Darcy's law is frequently used to model convection in porous material. This model was expanded by Brinkman (1947) and Chan and Barry (1970) by adding a viscous term for extremely permeable mediums. Since then, the Brinkman model has been widely applied. In 2003, Nazar et al. (2003) used the Keller-Box method to study mixed convection boundary-layer flow across a heated horizontal cylinder immersed in a porous material. They found that the Brinkman and mixed convection factors dictate skin friction and heat transmission, with bigger mixed convection values lowering both. By adding nanoparticles, Tham et al. (2016) further integrated the Brinkman and Buongiorno models and showed how the local Nusselt number is significantly reduced by Brinkman, Brownian motion, and thermophoresis. The role of porosity and elasticity in convection was highlighted by Kanafiah et al. (2022), who applied the Brinkman model to viscoelastic fluids and discovered that raising the Brinkman and viscoelastic parameters improves heat transmission.

To the best of our knowledge, no work has been reported since then that considers the Buongiorno (2006) nanofluid model with Brinkman flow to analyse mixed convective boundary layer flow past a horizontal circular cylinder incorporating viscoelastic effects. This work aims to address the existing gap. The governing equations are solved numerically using the Keller-Box method and the influence of the viscoelastic parameter, Lewis number, Brownian number, thermophoresis parameter and buoyancy ratio parameter on the coefficient of the skin friction, the local Nusselt number and the local Sherwood number are analysed and presented in tables and figures. For validation purposes, the present results are computed and compared with the results obtained by Kanafiah et al. (2021). The embedded mixed convection in the study of fluid flow was also considered by Alam et al. (2022) in the study of bio magnetic fluid.

2. METHODOLOGY

The research process is outlined in a flowchart. First, the equations, which are typically nonlinear partial differential equations, are made dimensionless. This is achieved by employing non-dimensional variables. A similarity transformation is subsequently employed to simplify the equations into a more tractable form. The resultant equations are resolved numerically via the Keller-Box method (KBM).

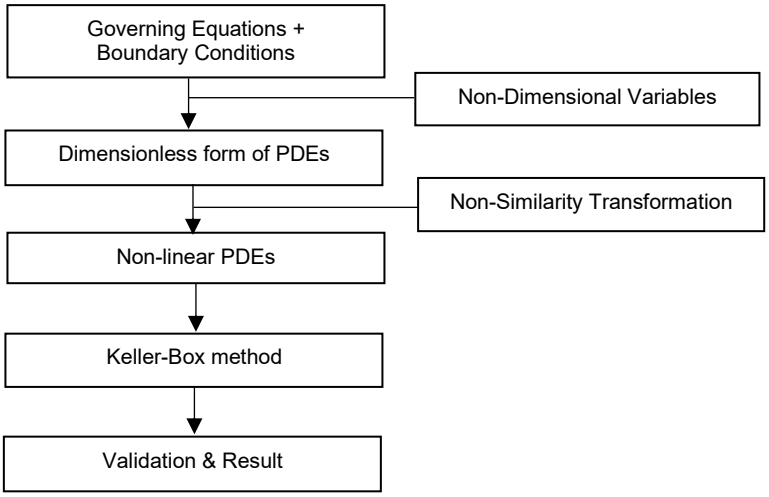

Figure 1. The Methodology Flow

The Keller-Box method is a numerical technique with a four-step process. The procedure begins by converting the governing PDEs into a first-order system. Subsequently, this system undergoes discretization using central finite differences. The obtained finite-difference equations are then linearized via the method of Newton and represented in a matrix-vector format. The final numerical solution is obtained by employing a block tridiagonal elimination technique. Around a horizontal circular cylinder of radius a, this study analyses the coupled convection flow of a nanofluid in a porous medium. Figure 2 shows that the x-axis is measured in the usual direction, whereas the y-axis is measured along the surface of the cylinder, starting at the lowest point of stagnation. The temperature of the surrounding fluid is believed to be constant, while the temperature of the cylinder's surface remains constant. Additionally, it is assumed that a steady stream is ascending vertically across the cylinder. Consider a porous material that possesses both porosity and permeability.

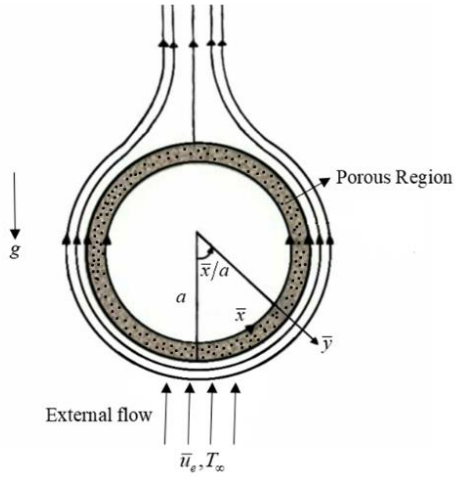

Figure 2. Fluid Flow Pattern

Given these assumptions, the equations are (Kanafiah et al., 2022; Tham et al., 2013)

$$\frac{\partial \bar{u}}{\partial \bar{x}} + \frac{\partial \bar{v}}{\partial \bar{y}} = 0 \tag{1}$$

$$\frac{\mu}{K}\bar{u} = \bar{u}_e \frac{\partial \bar{u}_e}{\partial \bar{x}} + \frac{\mu}{\phi}\frac{\partial^2 \bar{u}}{\partial \bar{y}^2} + k_0 \left[\begin{array}{l} \bar{u}\dfrac{\partial^3 \bar{u}}{\partial \bar{x}\partial \bar{y}^2} + \bar{v}\dfrac{\partial^3 \bar{u}}{\partial \bar{y}^3} - \\ \dfrac{\partial \bar{u}}{\partial \bar{y}}\dfrac{\partial^2 \bar{u}}{\partial \bar{x}\partial \bar{y}} + \dfrac{\partial \bar{u}}{\partial \bar{x}}\dfrac{\partial^2 \bar{u}}{\partial \bar{y}^2} \end{array} \right] + \left[\begin{array}{l} (1-C_\infty)\rho_{f\infty}\beta(T-T_\infty) - \\ (\rho_p - \rho_{f\infty})(C-C_\infty) \end{array} \right] g \sin\left(\frac{\bar{x}}{a}\right) \tag{2}$$

$$\bar{u}\frac{\partial T}{\partial \bar{x}} + \bar{v}\frac{\partial T}{\partial \bar{y}} = \alpha_m \frac{\partial^2 T}{\partial \bar{y}^2} + \tau \left[D_B \frac{\partial C}{\partial \bar{y}}\frac{\partial T}{\partial \bar{y}} + \frac{D_T}{T_\infty}\left(\frac{\partial T}{\partial \bar{y}}\right)^2 \right] \tag{3}$$

$$\frac{1}{\phi}\left(\bar{u}\frac{\partial C}{\partial \bar{x}}+\bar{v}\frac{\partial C}{\partial \bar{y}}\right)=D_B\frac{\partial^2 C}{\partial \bar{y}^2}+\frac{D_T}{T_\infty}\frac{\partial^2 T}{\partial \bar{y}^2} \tag{4}$$

where $\bar{u}$ and $\bar{v}$ represent velocity, T denotes temperature, C signifies the nanoparticle volume fraction, g indicates gravitational acceleration, α_m refers to the porous medium thermal diffusivity, ϕ represents porosity, μ is the dynamic viscosity of the fluid, ρ_f denotes fluid density, ρ_p signifies nanoparticle mass density, and β refers to the nanofluid's volumetric expansion coefficient. The coefficients included in Eq. (3) and Eq. (4) are the Brownian diffusion coefficient D_B, thermophoretic diffusion coefficient D_T and buoyancy ratio coefficient D_R.

The continuity equation, Eq. (1), is based on the principle of mass conservation, which asserts that the rate of mass flow into a system equals the rate of mass flow out of the system (Çengel and Ghajar, 2020). In the momentum equation, Eq. (2), the density of fluid as used in the momentum equation by Kanafiah et al. (2022) is now changed into the density of nanofluid as mentioned in Tham et al. (2013). The energy equation, Eq. (3), similarly incorporates the nanofluid term (the last term) that includes Brownian motion and the thermophoresis parameter as described by Buongiorno (2006). Unlike the Brinkman model of conventional fluid dynamics, this model has an additional equation which is the concentration equation Eq. (4), developed by Buongiorno (2006), which reflects the mass transfer of nanoparticles. All of these equations Eq. (1) – Eq. (4) are constrained by the boundary conditions (Kanafiah et al., 2022; Tham et al., 2013)

$$\begin{aligned}&\bar{v}=0,\quad \bar{u}=0,\quad T=T_w,\ C=C_w \text{ at } \bar{y}=0\\&\bar{u}\to\bar{u}_e(\bar{x}),\ \bar{v}\to 0,\ T\to T_\infty, C\to C_\infty \text{ as } \bar{y}\to\infty\end{aligned} \tag{5}$$

where $\bar{u}_e(\bar{x})$ is the external flow velocity and $\tau=\phi\left(\rho C_f/\rho C_p\right)$ with ρC_f is the fluid heat capacity and ρC_p is the nanoparticle material effective heat capacity.

The boundary layer approximations are defined as (Kanafiah et al., 2022; Tham et al., 2013)

$$\begin{aligned}&x=\bar{x}/a,\quad y=Pe^{1/2}(\bar{y}/a),\quad u=\bar{u}/U_\infty,\ v=Pe^{1/2}(\bar{v}/U_\infty),\theta=(T-T_\infty)/(T_w-T_\infty),\\&\varphi=\left(C-C_\infty\right)/\left(C_w-C_\infty\right),\ u_e(\bar{x})=\bar{u}_e(\bar{x})/U_\infty.\end{aligned} \tag{6}$$

with $Pe=U_\infty a/\alpha_m$ are substituted into Eq. (1) – Eq. (5) to obtain the equations

$$\frac{\partial u}{\partial x}+\frac{\partial v}{\partial y}=0 \tag{7}$$

$$\frac{\partial u}{\partial y}=\Gamma\frac{\partial^3 u}{\partial y^3}+k_1\left[u\frac{\partial^4 u}{\partial x\partial y^3}+\frac{\partial v}{\partial y}\frac{\partial^3 u}{\partial y^3}+v\frac{\partial^4 u}{\partial y^4}+\frac{\partial u}{\partial x}\frac{\partial^3 u}{\partial y^3}\right]+\left[\frac{\partial\theta}{\partial y}-Nr\frac{\partial\varphi}{\partial y}\right]\lambda\sin(x) \tag{8}$$

$$u\frac{\partial\theta}{\partial x}+v\frac{\partial\theta}{\partial y}=\frac{\partial^2\theta}{\partial y^2}+Nb\frac{\partial\varphi}{\partial y}\frac{\partial\theta}{\partial y}+Nt\left(\frac{\partial\theta}{\partial y}\right)^2 \tag{9}$$

$$Le\left(u\frac{\partial\varphi}{\partial x}+v\frac{\partial\varphi}{\partial y}\right)=\frac{\partial^2\varphi}{\partial y^2}+\frac{N_t}{N_B}\frac{\partial^2\theta}{\partial y^2} \tag{10}$$

and the boundary conditions Eq. (5) become

$$\begin{aligned}&u=0,\quad v=0,\quad \theta=1 \quad \text{at } \bar{y}=0\\&u\to u_e, v\to 0,\quad \theta\to 0 \quad \text{as } \bar{y}\to\infty\end{aligned} \tag{11}$$

where $u_e(x)=\sin x$. The definitions for the key parameters in the model are as follows:

- Brinkman parameter (Γ): Measures the ratio of thermal energy produced by viscous dissipation to thermal energy conveyed through molecular conduction.

- Lewis number (Le): The ratio of thermal diffusivity to mass diffusivity, important for processes with simultaneous heat and mass transfer.
- Mixed convection parameter (λ): Indicates the relative importance of natural convection (due to buoyancy forces) compared to forced convection.
- Buoyancy ratio parameter (Nr): Denotes the ratio of buoyant force resulting from concentration gradients to buoyancy force arising from temperature gradients.
- Brownian motion parameter (Nb): Characterizes the nanoparticles random movement within the fluid due to collisions with fluid molecules, which enhances energy transport.
- Thermophoresis parameter (Nt): Measures the displacement of particles in a fluid induced by a temperature gradient, wherein particles transition from warmer to cooler areas.

$$\Gamma = \frac{kPe}{\phi a^2}, Le = \frac{\alpha_m}{\phi D_B}, \lambda = \frac{k\rho g\beta}{U_\infty \mu}, \tag{12}$$
$$Nb = \frac{\phi\left(\rho C_p\right) D_B \left(C_w - C_\infty\right)}{\left(\rho C_f\right)\alpha_m}, Nt = \frac{\phi\left(\rho C_p\right) D_T \left(T_w - T_\infty\right)}{\left(\rho C_f\right)\alpha_m T_\infty}, Nr = \frac{\left(\rho_p - \rho_{f\infty}\right)\left(C_w - C_\infty\right)}{\rho_{f\infty}\beta\left(T_w - T_\infty\right)\left(1 - C_\infty\right)}$$

From Eq. (12), it can be seen here that the values of Nb and Nt depend on the coefficients D_B and D_T respectively. While the two coefficients are contingent upon the Boltzmann's constant (k_B), nanofluid temperature (T), nanoparticle diameter (d_p), nanofluid density (ρ), proportionality factor (β_f) and the relations are $D_B = \frac{k_B T}{3\pi\mu d_p}$, $D_T = \beta_f \frac{\mu}{\rho}\phi$ (Buongiorno, 2006). This study exclusively examines the models and their potential functionalities; therefore, we will consider a range of values for Nb, Nt, and Nr in our analysis. These values do not correspond to any specific materials, as a detailed computation of Nb, Nt, and Nr is required for particular materials.

The non-dimensional form of Eq. (7) – Eq. (11) are then converted to solvable equations by employing non-similarity variables

$$\psi = x f(x,y),\ \theta = \theta(x,y),\ \varphi = \varphi(x,y),\ u = \frac{\partial\psi}{\partial y},\ v = -\frac{\partial\psi}{\partial x}, \tag{13}$$

with ψ represents the function of stream. The transformed and solvable equations are shown below:

$$f' - \Gamma f''' - k_1\left[2ff''' - ff^{(4)} - \left(f''\right)^2\right] - \frac{\left[\theta - Nr\varphi\right]\lambda\sin\left(x\right)}{x} - \frac{\sin x}{x} \tag{14}$$
$$= k_1 x\left[f'\frac{\partial f'''}{\partial x} - \frac{\partial f}{\partial x}f^{(4)} + \frac{\partial f'}{\partial x}f''' - \frac{\partial f''}{\partial x}f''\right]$$
$$\theta'' + f\theta' + Nb\varphi'\theta' + Nt\left(\theta'\right)^2 = x\left[f'\frac{\partial\theta}{\partial x} - \frac{\partial f}{\partial x}\theta'\right] \tag{15}$$
$$\varphi'' + \frac{N_t}{N_B}\theta'' + Lef\varphi' = xLe\left[f'\frac{\partial\varphi}{\partial x} - \frac{\partial f}{\partial x}\varphi'\right] \tag{16}$$

subjected to boundary conditions

$$f\left(x,0\right) = 0, f'\left(x,0\right) = 0, \theta\left(x,0\right) = 1,\ \varphi\left(x,0\right) = 1 \tag{17}$$
$$f'\left(x,\infty\right) \to \frac{\sin x}{x}, f''\left(x,\infty\right) \to 0,\ \theta\left(x,\infty\right) \to 0, \varphi\left(x,\infty\right) \to 0$$

It is observed that when Nb, Nt, Nr, and Le are diminished to zero, the case study reverts to the scenario examined by Kanafiah et al. (2022), who analysed this model using the Brinkman-viscoelastic framework. Furthermore, the case study is streamlined to the mixed convective boundary

layer flow of a nanofluid around a horizontal circular cylinder within fluid-saturated porous media when the viscoelastic parameter k_1 is zero, aligning with the findings of Tham et al. (2013). In fluid mechanics and convective heat transfer, numerous dimensionless parameters are involved. The dimensionless parameters pertinent to this subject are the skin friction coefficient C_f, the local Nusselt number Nu_x, and the local Sherwood number Sh_x. Nusselt number Nu_x is a dimensionless number that represents the convection heat transfer rate (Çengel and Ghajar, 2020). On the other hand, the skin friction coefficient C_f is a dimensionless quantity utilised to characterise boundary layer behaviour. A higher C_f signifies a reduced boundary layer, resulting in enhanced heat transfer (Harun et al., 2014). The Sherwood number, denoted as Sh_x, is a dimensionless number that signifies mass transfer. These three numbers pertain to distinct phenomena, although collectively they elucidate the processes involved in heat and mass transmission and they are described as follows:

$$C_f = \frac{\tau_w}{\rho U_\infty{}^2},\ Nu_x = \frac{aq_w}{k\left(T_w - T_\infty\right)},\ Sh_x = \frac{aj_w}{D_B\left(C_w - C_\infty\right)} \tag{18}$$

where τ_w, q_w and j_w are shear stress of the wall, the heat flux of the wall and the heat flux of the mass from the surface of the cylinder, respectively, as shown in

$$\tau_w = \mu_f\left(\frac{\partial \overline{u}}{\partial \overline{y}}\right) + k_0\left(\overline{u}\frac{\partial^2 \overline{u}}{\partial \overline{x}\partial \overline{y}} + \overline{v}\frac{\partial^2 \overline{u}}{\partial \overline{y}^2} + 2\frac{\partial \overline{u}}{\partial \overline{x}}\frac{\partial \overline{u}}{\partial \overline{y}}\right),\ q_w = -k_m\left(\frac{\partial T}{\partial \overline{y}}\right),\ j_w = -D_B\left(\frac{\partial C}{\partial \overline{y}}\right) \tag{19}$$

where k_m is the porous medium effective thermal conductivity. Substituting variables Eq. (6) and Eq. (13) into Eq. (18) and Eq. (19) gives

$$\left(Pe^{\frac{1}{2}} / \mathrm{Pr}\right)C_f = xf''(0), Pe^{-\frac{1}{2}}Nu_x = -\theta'(0), Pe^{-\frac{1}{2}}Sh_x = -\varphi'(0). \tag{20}$$

where $\mathrm{Pr} = \upsilon_f / \alpha_m$ is the porous medium Prandtl number.

3. RESULTS AND DISCUSSION

To assess the impact of different parameters, equations Eq. (14-16) were numerically solved subject to boundary conditions Eq. (17). The Keller-Box method was applied, in which the Newton's linearisation technique was used to solve the equations for various parameter values of λ, Nb, Nt, and Nr at predetermined streamwise places. This methodology is based on the techniques described by Cebeci and Bradshaw (1984). The skin friction coefficient (C_f), the local Sherwood number (Sh_x), and the local Nusselt number (Nu_x) are computed as well as nanoparticle volume fraction ($\varphi(y)$), temperature ($\theta(y)$), and velocity ($f'(y)$) profiles. These values and profiles were calculated for the specified range of parameters involved at various streamwise locations: buoyancy ratio parameter, Brinkman parameter, Lewis number, Brownian number, mixed convection parameters, and thermophoresis parameter. In order to validate the findings, the results of $f''(0)$ and $-\theta'(0)$ when the value of $Nr = Nt = 0, Nb \approx 0(0.000001)$, $k_1 = 0.01$, $Le = 2$ and $\Gamma = 0.1$ of this study are compared with the results documented and published in Kanafiah et al. (2021) as publicised in Table 1. From the output, it can be seen that there is a total agreement in the result that validates the suggested calculation correctness.

This research considers the viscoelastic parameter k_1 to examine the effects of viscosity and elasticity qualities. Consequently, the value of k_1 must exceed zero to demonstrate these characteristics. Tables 3, 4, and 5 shows the value of skin friction coefficient, local Nusselt number, and Sherwood number for several values of k_1.

Table 1. Comparison for values of $f''(0)$ and $-\theta'(0)$

λ	**Kanafiah et al. (2021)**		**Current**	
	$f''(0)$	$-\theta'(0)$	$f''(0)$	$-\theta'(0)$
0.1	3.1752	0.6623	3.1752	0.6623
0.2	3.3972	0.6747	3.3927	0.6747
0.3	3.6068	0.6866	3.6068	0.6866
0.4	3.8175	0.6980	3.8175	0.6980
0.5	4.0252	0.7089	4.0252	0.7089
0.6	4.2300	0.7195	4.2299	0.7195
0.7	4.4317	0.7297	4.4317	0.7297
0.8	4.6310	0.7396	4.6310	0.7396
0.9	4.8276	0.7491	4.8276	0.7491
1.0	5.0218	0.7583	5.0218	0.7583

Table 2. Comparative study

Momentum Equation	**With Cases**
Current	
$f' - \Gamma f''' - k_1\left[2ff''' - ff^{(4)} - (f'')^2\right] - \frac{[\theta - Nr\varphi]\lambda\sin(x)}{x} - \frac{\sin x}{x}$	$Nr = 0, k_1 = 0$
$= k_1 x\left[f'\frac{\partial f'''}{\partial x} - \frac{\partial f}{\partial x}f^{(4)} + \frac{\partial f'}{\partial x}f''' - \frac{\partial f''}{\partial x}f''\right]$	
Kanafiah et al. (2022)	
$f' - \Gamma f''' - k_1\left[2ff''' - ff^{(4)} - (f'')^2\right] - (1+\lambda\theta)\frac{\sin x}{x}$	$k_1 = 0$
$= k_1 x\left[f'\frac{\partial f'''}{\partial x} - \frac{\partial f}{\partial x}f^{(4)} + \frac{\partial f'}{\partial x}f''' - \frac{\partial f''}{\partial x}f''\right]$	
Tham et al. (2013)	
$f' - \Gamma f''' - \frac{[\theta - Nr\varphi]\lambda\sin(x)}{x} - \frac{\sin x}{x} = 0$	$Nr = 0$
Nazar et al. (2003)	-
$f' - \Gamma f''' - (1+\lambda\theta)\frac{\sin x}{x} = 0$	

Table 3. The skin friction coefficient $\left(Pe^{\frac{1}{2}}/\Pr\right)C_f$ for $\Gamma = 0.1$, $\lambda = 1$, $Le = 2$, $Nb = 0.5$, $Nr = 0.5$ and $Nt = 0.5$ for several k_1 values

x	k_1		
	8	**10**	**12**
0.2	0.085105	0.076316	0.069794
0.4	0.169324	0.151841	0.138865
0.6	0.251787	0.225800	0.206509
0.8	0.331646	0.297434	0.272035
1.0	0.408076	0.366009	0.334772
1.2	0.480287	0.430819	0.394080
1.4	0.547526	0.491195	0.449346
1.6	0.609090	0.546509	0.500002
1.8	0.664326	0.596182	0.545519
2.0	0.712641	0.639687	0.585421
2.2	0.753505	0.676555	0.619280
2.4	0.786454	0.706377	0.646728
2.6	0.811092	0.728805	0.667454

Table 4. The local Nusselt number $Pe^{-\frac{1}{2}}Nu_x$ for $\Gamma = 0.1$, $\lambda = 1$, $Le = 2$, $Nb = 0.5$, $Nr = 0.5$ and $Nt = 0.5$ for several k_1 values

x	k_1		
	8	**10**	**12**
0.2	0.242570	0.235788	0.230433
0.4	0.241881	0.235154	0.229846
0.6	0.240729	0.234080	0.228832
0.8	0.239108	0.232568	0.227404
1.0	0.237013	0.230614	0.225559
1.2	0.234436	0.228213	0.223392
1.4	0.231361	0.225352	0.220595
1.6	0.227772	0.222019	0.217457
1.8	0.223643	0.218193	0.213861
2.0	0.218941	0.213849	0.209786
2.2	0.213620	0.208952	0.205206
2.4	0.207613	0.203451	0.200081
2.6	0.200822	0.197278	0.194356

Table 5. The Sherwood number $Sh_x Pe^{-\frac{1}{2}}$ for $\Gamma = 0.1$, $\lambda = 1$, $Le = 2$, $Nb = 0.5$, $Nr = 0.5$ and $Nt = 0.5$ for several k_1 values

x	k_1		
	8	**10**	**12**
0.2	0.529898	0.51525	0.50369
0.4	0.528335	0.513818	0.502362
0.6	0.525816	0.511471	0.500148
0.8	0.522288	0.508179	0.497038
1.0	0.517734	0.503931	0.493024
1.2	0.512133	0.498710	0.488095
1.4	0.505456	0.492494	0.482232
1.6	0.497666	0.485254	0.475412
1.8	0.488711	0.476949	0.467600
2.0	0.478521	0.467525	0.458754
2.2	0.467001	0.456909	0.448814
2.4	0.454014	0.444998	0.437701
2.6	0.439361	0.431648	0.425302

The numerical results clearly show that when the viscoelastic parameter goes up, the skin friction coefficient, $\left(Pe^{\frac{1}{2}}/\Pr\right)C_f$, goes down by a large amount. This is because elastic forces in the fluid limit the diffusion of momentum near the cylinder surface. This aligns with the expected behaviour of viscoelastic fluids, where elasticity minimizes deformation and reduces velocity gradients near the boundary (Zokri et al., 2020). When the flow slows down near the wall and thickens the thermal boundary layer, it results in a smaller temperature gradient, and therefore, the local Nusselt number is lowered. As for the Sherwood number, viscoelasticity makes mass transfer less effective, which makes the Sherwood number smaller. For a better view, the effect of the viscoelastic parameter on the skin friction coefficient $\left(Pe^{\frac{1}{2}}/\Pr\right)C_f$ and on the local Nusselt number $Pe^{-\frac{1}{2}}Nu_x$ are illustrated in Figure 3(a) and 3(b).

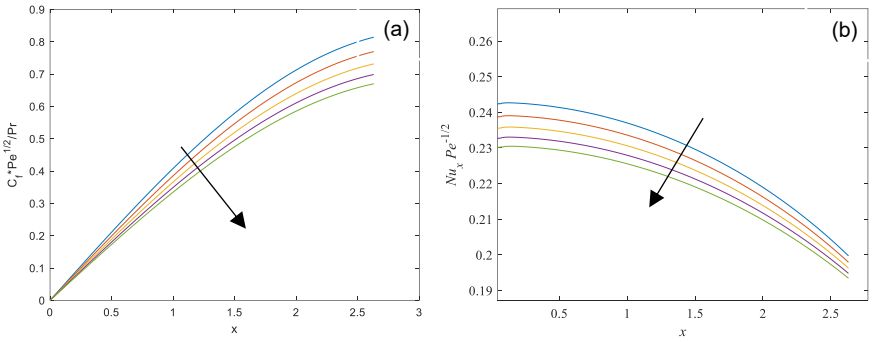

Figure 3. Effect of $k_1 = 8,9,10,11,12$ on (a) skin friction coefficient $\left(Pe^{\frac{1}{2}}/\Pr\right)C_f$ and on (b) local Nusselt number $Pe^{-\frac{1}{2}}Nu_x$ with x for $\Gamma = 0.1$, $\lambda = 1$, $Le = 2$, $Nb = 0.5$, $Nr = 0.5$ and $Nt = 0.5$

Figure 4 shows the behaviour of the velocity profiles $f'(y)$ and temperature profiles $\theta(y)$ for various values of the viscoelastic parameter at $x = 0$ for $\Gamma = 0.1$, $\lambda = 1$, $Le = 2$, $Nb = 0.5$, $Nr = 0.5$ and $Nt = 0.5$. It is observed in Figure 4(a) that the velocity profiles $f'(y)$ decrease as k_1 increases. It is also noticed in Figure 4(b) that temperature profiles decrease with an increase in the value of k_1.

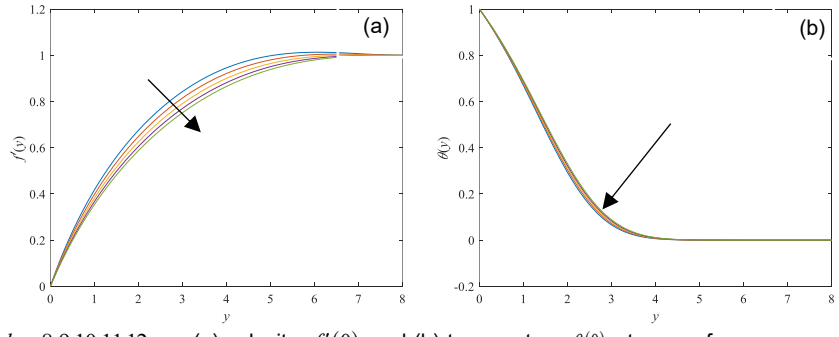

Figure 4. Effect of $k_1 = 8,9,10,11,12$ on (a) velocity $f'(0)$ and (b) temperature $\theta(0)$ at $x = 0$ for $\Gamma = 0.1$, $\lambda = 1$, $Le = 2$, $Nb = 0.5$, $Nr = 0.5$ and $Nt = 0.5$

Figure 5 shows the effect of k_1 on the behaviour of the nanoparticle volume fraction profiles $\varphi(y)$ indicating that the thickness of the mass fraction boundary layers decreases with increasing values k_1.

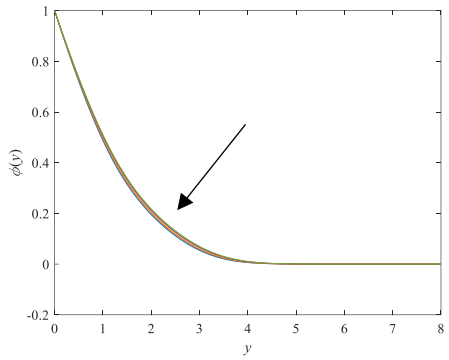

Figure 5. Effect of $k_1 = 8,9,10,11,12$ on nanoparticle volume fraction $\varphi(0)$ at $x = 0$ for $\Gamma = 0.1$, $\lambda = 1$, $Le = 2$, $Nb = 0.5$, $Nr = 0.5$ and $Nt = 0.5$

Figure 6 and 7 show the variation of the skin friction coefficient $\left(Pe^{\frac{1}{2}}/\Pr\right)C_f$ and local Nusselt number $Pe^{-\frac{1}{2}}Nu_x$ versus the Brownian number Nb and the thermophoresis parameter Nt. In Figure 6, the increase in the value Brownian number increases the skin friction coefficient but decreases the local Nusselt number. The same goes to the thermophoresis parameter as shown in Figure 7. The local Nusselt number diminishes as the parameters Nb and Nt grow due to the augmented volume of nanoparticles that are moving away from the wall. As a result, the rate of thermal transfer diminishes.

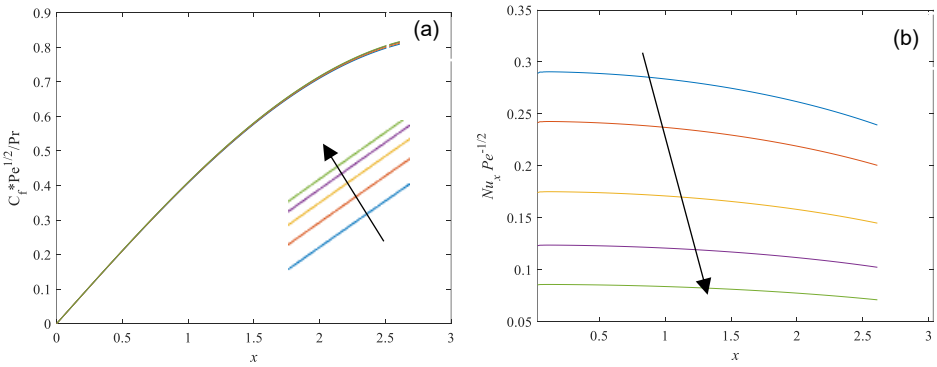

Figure 6. Effect of $Nb = 0.2,0.5,1,1.5,2.0$ on (a) $\left(Pe^{\frac{1}{2}}/\Pr\right)C_f$ and (b) $Pe^{-\frac{1}{2}}Nu_x$ with x for $\Gamma = 0.1$, $\lambda = 1$, $Le = 2$, $k_1 = 8$, $Nr = 0.5$ and $Nt = 0.5$

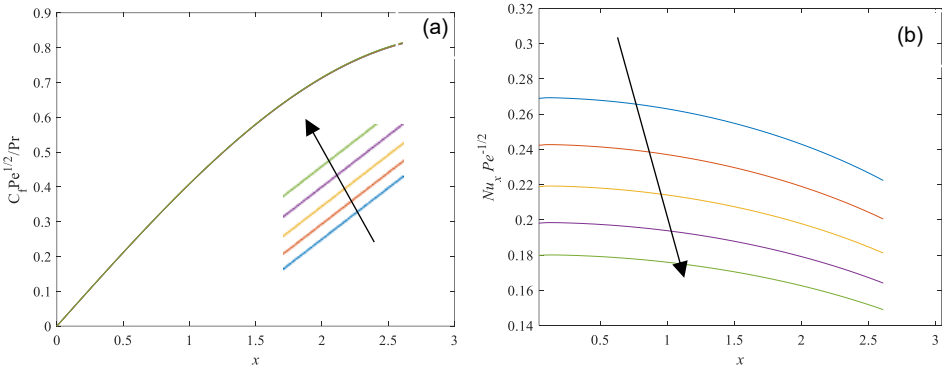

Figure 7. Effect of $Nt = 0.25,0.5,0.75,1,1.25$ on (a) $\left(Pe^{\frac{1}{2}}/\Pr\right)C_f$ and (b) $Pe^{-\frac{1}{2}}Nu_x$ with x for $\Gamma = 0.1$, $\lambda = 1$, $Le = 2$, $k_1 = 8$, $Nr = 0.5$ and $Nb = 0.5$

4. CONCLUSION

The research of a Brinkman-viscoelastic nanofluid using Buongiorno model flowing over a circular cylinder with horizontal orientation by considering a constant wall temperature boundary condition is presented. The model's governing equations are reduced to a solvable form by applying the non-dimensional and non-similarity variables. The numerical solutions are checked against prior work that used the Keller-Box method to confirm their accuracy. This study shows that the viscoelastic properties of a fluid increase the skin friction but decrease the local Nusselt number. This means that the wall transfers heat to the fluid more slowly or it can be said that a viscoelastic fluid moves less heat away from the wall. So, it is not always true that a fluid's viscoelastic properties make the convective heat transfer rate faster. Regarding nanofluids, their nanoparticles do not always enhance heat transmission. It is dependent on both the volume fraction and the thermal conductivity of the nanoparticles. As for the recommendations, one possible approach is to decrease the concentration of polymer-based viscoelastic additives or select fluids with lower elasticity. Additionally, we could employ nanofluids containing high-conductivity particles or consider diluting multiple types of particles within the fluid to create a hybrid nanofluid. Since the Buongiorno model is being utilized, these are expressed in terms of the values of Nb (Brownian motion parameter), Nr (buoyancy ratio parameter), and Nt (thermophoresis parameter). With various nanoparticles employed, distinct values of Nb, Nt and Nr need to be applied. So, for further analysis, it is recommended to examine these values in detail as outlined by Buongiorno (2006).

ACKNOWLEDGEMENT
Financial support (Grant RDU253301) was provided by UMPSA. The writers would like to extend their gratitude to UiTM Kelantan and UTeM for their valuable advice and assistance.

CONFLICT OF INTEREST
No conflict of interest.

AUTHOR CONTRIBUTION
Farahanie Fauzi, Siti Farah Haryatie Mohd Kanafiah: Conceptualization and writing original draft; Nurizzatul Atikha Rahmat, Abdul Rahman Mohd Kasim: Investigation on results and discussion; Adeshina Taofeeq Adeosun, Nurul Amira Zainal, Livia Owen: Methodology; Farahanie Fauzi, Abdul Rahman Mohd Kasim: Formal analysis, review, editing and supervision.

DATA AVAILABILITY
All supporting data relevant to the results of this study are included in the article.

DECLARATION OF GENERATIVE AI
Not applicable.

ETHICS
Not applicable.

REFERENCES

Ahmed SA, Ozkaymak M, Sözen A, Menlik T, Fahed A. (2018). Improving car radiator performance by using TiO_2-water nanofluid. *Engineering Science and Technology, an International Journal*, 21, 996-1005. doi:10.1016/j.jestch.2018.07.008

Alam MJ, Talukder MG, Tzirtzilakis E, Ferdows M. (2022). Mixed convection flow and heat transfer of biomagnetic fluid with magnetic/non-magnetic particles due to a stretched cylinder in the presence of a magnetic dipole. *Proceedings of International Exchange and Innovation Conference on Engineering & Science*, 8, 76-83. doi:10.5109/5909065

Ali M, El-Leathy AM, Al-Sofyany Z. (2014). The effect of nanofluid concentration on the cooling system of vehicles radiator. *Advances in Mechanical Engineering*, 6, 962510. doi:10.1155/2014/962510

Aziz LA, Kasim ARM, Salleh MZ. (2019). Development on mathematical model of convective boundary layer flow of viscoelastic fluid with microrotation effect under constant wall temperature thermal condition over a bluff body. *ASM Science Journal*, 12, 86-90.

Brinkman HC. (1949). A calculation of the viscous force exerted by a flowing fluid on a dense swarm of particles. *Flow, Turbulence and Combustion*, 1, 27-34. doi:10.1007/BF02120313

Buongiorno J. (2006). Convective transport in nanofluids. *Journal of Heat Transfer*, 128, 240-250. doi:10.1115/1.2150834

Cebeci T, Bradshaw P. (1984). Uncoupled laminar duct flows. In Physical and Computational Aspects of Convective Heat Transfer, 124-149. Springer Berlin Heidelberg. doi:10.1007/978-3-662-02411-9_5

Çengel YA, Ghajar AJ. (2020). Heat and mass transfer: Fundamentals & applications. McGraw Hill Education.

Chan BKC, Barry JM. (1970). Natural convection in enclosed porous media with rectangular boundaries. *Journal of Heat Transfer*, 92(1), 21-27. doi:10.1115/1.3449641

Dey S, Ibtida T, Roy C, Sakib N. (2020). Difference between non-Newtonian Carreau and Casson blood viscosity models to predict hemodynamics in idealized eccentric arterial stenosis: Large eddy simulation modeling. *Proceedings of International Exchange and Innovation Conference on Engineering & Sciences*, 6, 249-257. doi:10.5109/4102499

Elsheikh AH, Sharshir SW, Mostafa ME, Essa FA, Ahmed Ali MK. (2018). Applications of nanofluids in solar energy: A review of recent advances. *Renewable and Sustainable Energy Reviews*, 82, 3483-3502. doi:10.1016/j.rser.2017.10.108

Harun Z, Syafiq M, Rasani MR, Abdullah S, Zulkifli R, Mohd Faizal Wan Mahmood W, Ghazali MJ, Azhari CH, Radzi Abu Mansor M, Abidin ZZ, Abbas AA. (2014). Skin friction coefficient and boundary layer trend on UKM Aster i-Bond. *Applied Mechanics and Materials*, 629, 450-455. doi:10.4028/www.scientific.net/AMM.629.450

Hussein AK. (2016). Applications of nanotechnology to improve the performance of solar collectors - Recent advances and overview. *Renewable and Sustainable Energy Reviews*, 62, 767-792. doi:10.1016/j.rser.2016.04.050

Ingham DB, Pop I. (1998). Transport phenomena in porous media. Pergamon.

Kanafiah SFHM, Kasim ARM, Zokri SM, Arifin NS. (2021). Numerical investigation at lower stagnation point flow over a horizontal circular cylinder of Brinkman-viscoelastic fluid. *Journal of Advanced Research in Fluid Mechanics and Thermal Sciences*, 87, 56-65. doi:10.37934/arfmts.87.2.5665

Kanafiah SFHM, Kasim ARM, Zokri SM, Arifin NS. (2022). Non-similarity solutions of non-Newtonian Brinkman-viscoelastic fluid. *Mathematics*, 10. doi:10.3390/math10122023

Kumar A, Hassan MA, Chand P. (2020). Heat transport in nanofluid coolant car radiator with louvered fins. *Powder Technology*, 376, 631-642. doi:10.1016/j.powtec.2020.08.047

Li J, Zhang X, Xu B, Yuan M. (2021). Nanofluid research and applications: A review. *International Communications in Heat and Mass Transfer*, 127. doi:10.1016/j.icheatmasstransfer.2021.105543

Mahat R, Januddi F, Shafie S. (2020). Numerical solutions of mixed convection flow past a horizontal circular cylinder with viscous dissipation in viscoelastic nanofluid. *Journal of Advanced Research in Micro and Nano Engineering*, 1(1) 24-37.

Nazar R, Amin N, Pop I. (2003). Mixed convection boundary-layer flow from a horizontal circular cylinder in micropolar fluids: Case of constant wall temperature. *International Journal of Numerical Methods for Heat and Fluid Flow*, 13, 86-109. doi:10.1108/09615530310456778

Pérez-Reyes I, Vargas-Aguilar RO, Pérez-Vega SB, Ortiz-Pérez AS. (2018). Applications of viscoelastic fluids involving hydrodynamic stability and heat transfer. *Polymer Rheology*, 29. doi:10.5772/intechopen.76122

Tham L, Nazar R, Pop I. (2013). Mixed convection boundary layer flow past a horizontal circular cylinder embedded in a porous medium saturated by a nanofluid: Brinkman model. *Journal of Porous Media*, 16, 5. doi:10.1615/JPorMedia.v16.i5.50

Tham L, Nazar R, Pop I. (2016). Mixed convection flow over a horizontal circular cylinder with constant heat flux embedded in a porous medium filled by a nanofluid: Buongiorno-Darcy model. *Heat and Mass Transfer*, 52, 1983-1991. doi:10.1007/s00231-015-1720-2

Zokri SM, Arifin NS, Kasim ARM, Salleh MZ. (2020). Flow of Jeffrey fluid over a horizontal circular cylinder with suspended nanoparticles and viscous dissipation effect: Buongiorno model. *CFD Letters*, 12, 1-13. doi:10.37934/cfdl.12.11.113